TITLE: Design of the Telescope Simulator imaging mirror

DISTRIBUTION

D Smith (RAL)
B Swinyard (RAL)
M Caldwell (RAL)
P Gray (RAL)
T Grundy (RAL)
M Ferlet (RAL)

CHANGE RECORD

ISSUE	SECTION	REASON FOR CHANGE
1.0		First draft of the document (23/03/01).
2.0		Update of R_{SM} and related mirror dimensions after SPIRE Telescope Simulator internal meeting at RAL (11/05/01) and addition of section 6.
3.0		Addition of section 5.3 on mechanical design and references updated (27/0701).

CONTENTS

APPLICABLE AND REFERENCE DOCUMENTS

RD1 Duncan et al., "Long wavelength (sub-mm) telescope simulator", Infrared Phys. 34-1 (1993)
RD2 SPIRE-Telescope simulator optical design, SPIRE-RAL-NOT 000622 (08/05/2001)
RD3 SPIRE-Telescope simulator requirements specification.
RD4 Martin D.H, "Long-wave optics", IEEE Trans. MTT 41-10 (1993).
RD5 SPIRE-Feedhorn focus positions, SPIRE-RAL-NOT 000566 (10/01/2001)
RD6 Murphy J.A., "Distortion of a simple gaussian beam on reflection from off-axis ellipsoidal mirrors", Int. J. Inf. Mm. Waves 8-9 (1987).
RD7 "Mirror M2, Telescope Simulator" mechanical drawing (ref. 1-KG-0720-500-AA).
RD8 SPIRE-Set-up and alignment procedure for the Telescope Simulator imaging mirror, SPIRE-RAL-NOT 000734 (02/07/2001)

1. Introduction

This note aims at presenting some practical solutions for the problem of 1:1 imaging between the source and the detector, giving recommendations for an adapted imaging mirror for the telescope simulator experiment, after taking into account the optical performances required as well as the manufacturing constraints.

2. Case of a mirror with biconic (ellipsoidal/spherical) surface

In the description of a previous telescope simulator in far-infrared range (RD1), a spherical mirror was used off-axis. This leads to degradation of imaging performances as it introduces aberrations.

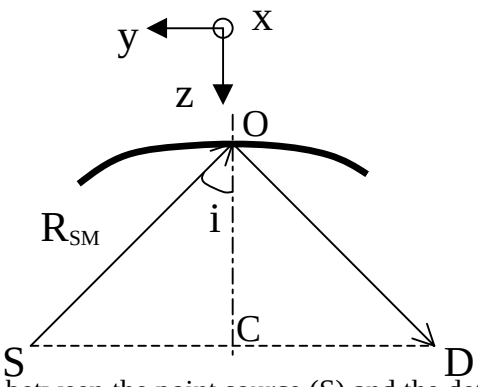

In order to have perfect imaging between the point source (S) and the detector (D), these points have to be located at the foci of an elliptically curved (in the plane yz) mirror. With an angle of incidence i for the incident beam at the mirror vertex O, the eccentricity e_y is given by $e_y=\tan(i)=\sqrt{K_y}$ where K_y is the conic constant. In order to adapt the radius of curvature R_y to the wavefront radius of curvature given by the specified distance $SO=R_{SM}$, one needs to have $R_y=R_{SM}*\sqrt{K_y+1}=R_{SM}/\cos(i)$. In the xz plane, the mirror can be just taken spherical ($K_x=0$) with its centre of curvature in C. Therefore the radius of curvature R_x is given by $R_x=R_{SM}*\cos(i)$. Applying these parameters at 45deg of incidence, and with R_{SM}=1980.8 mm[1], we obtain $K_x=0$, $K_y=1$, R_x=1400.64 mm, R_y=2801.29 mm.

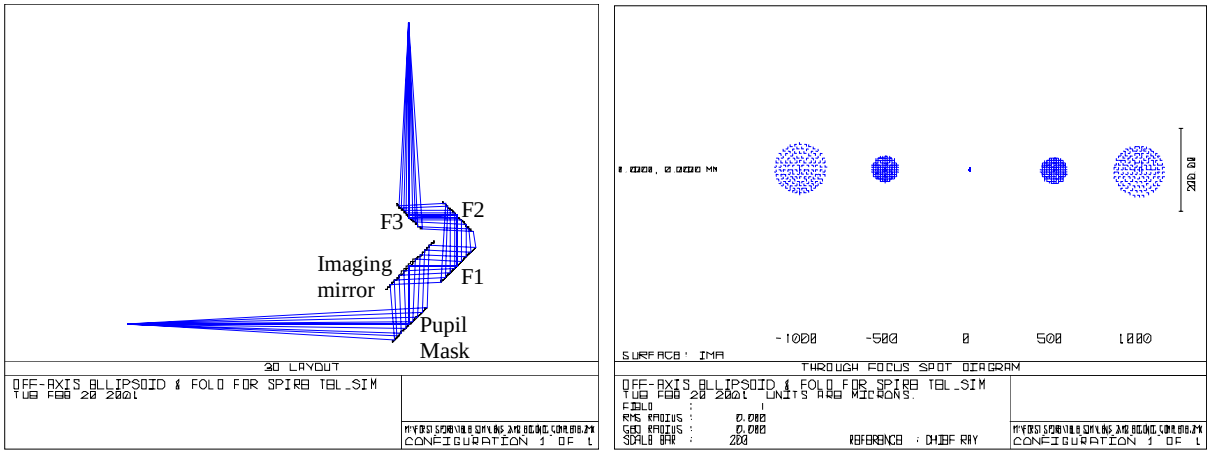

Figure 1: Zemax ray-tracing layout (yz plane) and spot diagrams around image surface for a test configuration

[1] This value for R_{SM} was determined from the study of constraints on the entire telescope simulator system layout (see RD2).

In Fig. 1, one can notice the quality of the image at the conjugate point of the point source. The displayed configuration uses the above values for the surface definition and R_{SM}. It also includes the mask (beam stop with an entrance pupil diameter set to ~181.1 mm at 1573.5 mm from the source in order to simulate a system with F# ~8.68 as required in RD3), the imaging mirror under 45deg of incidence, and a set of 3 fold mirrors (F1, F2 and F3). Longitudinal defocusing by ±1 mm gives rise to a spot size no larger than 100 μm (rms radius).

3. Case of a mirror with a toroidal surface

We consider now a surface having still 2 different radii of curvature R_x and R_y but spherical in both planes with $K_x=K_y=0$. The radii of curvature are still defined by the same definitions as above: $R_x=R_{SM}*\cos(i)$ and $R_y=R_{SM}/\cos(i)$. On-axis (normal incidence, i=0), the surface becomes simply spherical with $R_x=R_y=R_{SM}$ giving perfect imaging of the source. But practically, one has to use the mirror off-axis, introducing aberrations partially, not entirely attenuated by the toroidal surface shape. With i=20deg, R_x=1861.35 mm and R_y=2107.93 mm. Consequently, the beam size on the mirror is then reduced (extension to ~240 mm in diameter) when compared to the 45deg case.

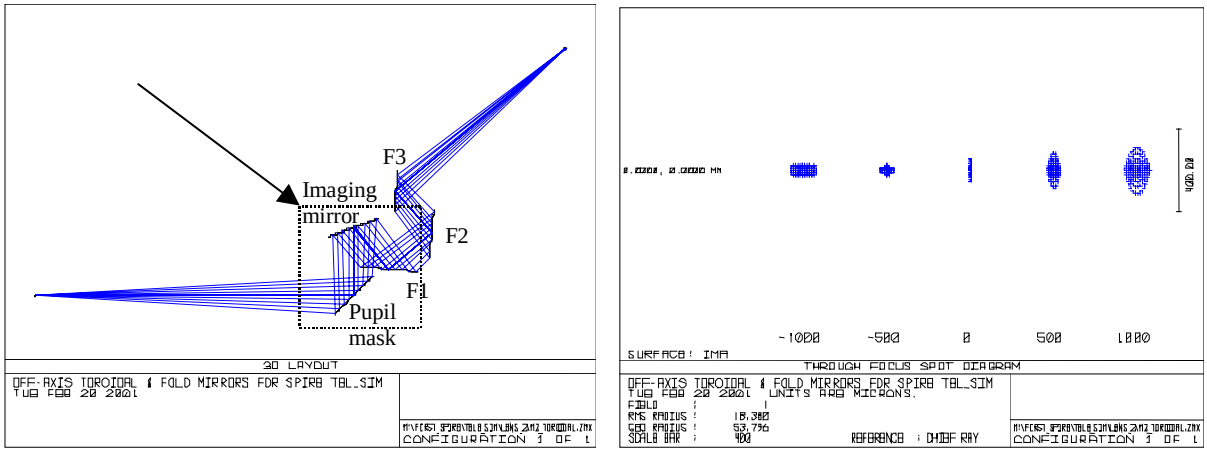

Figure 2: Zemax ray-tracing layout (yz plane) and spot diagrams for a second configuration (i=20deg)

In Figure 2, the effects of aberrations are seen on the spot diagrams. At the conjugate point, the beam has a linear extension and a better focus point can be chosen within ~0.5 mm max before the conjugate point position. Although including some aberrations, the image of the point source remains smaller than 100 μm in that configuration. But the large radial size of the beam and the constraints on the mask-mirror and mirror-first fold mirror distances can produce practical problems such as the incident beam impinging on the mirror may be partially diffracted by the first fold mirror edge (see dashed box in Fig 2, left). Even if the mask is used in transmission, there is necessity to increase either the mirror-F1 distance (set to 300 mm here) or the rotation angle (about x) for the imaging mirror so as to separate the incident and the reflected beam of the imaging mirror. As the distance between the mirrors can not be changed by much (± 50 mm max for the beam control), the angle i should be increased and consequently the mirror size as well. In Figure 3, a configuration with i=35deg is displayed (mask used in transmission) where it can be seen that the incident beam on the imaging mirror will still be close to the edge of the first fold mirror F1. Therefore due to beam size and system geometry constraints, i needs to be larger than 35deg (and smaller than 45deg to keep the whole experimental set-up in a reasonable surface area). But spot pattern with the toroidal mirror degrades rapidly as i is increased. At

35deg, the best focus would be mostly located ~2±1 mm away (longitudinally shifted) along the optical path and its rms size would already reach ~200 μm (getting even larger at i=45deg).

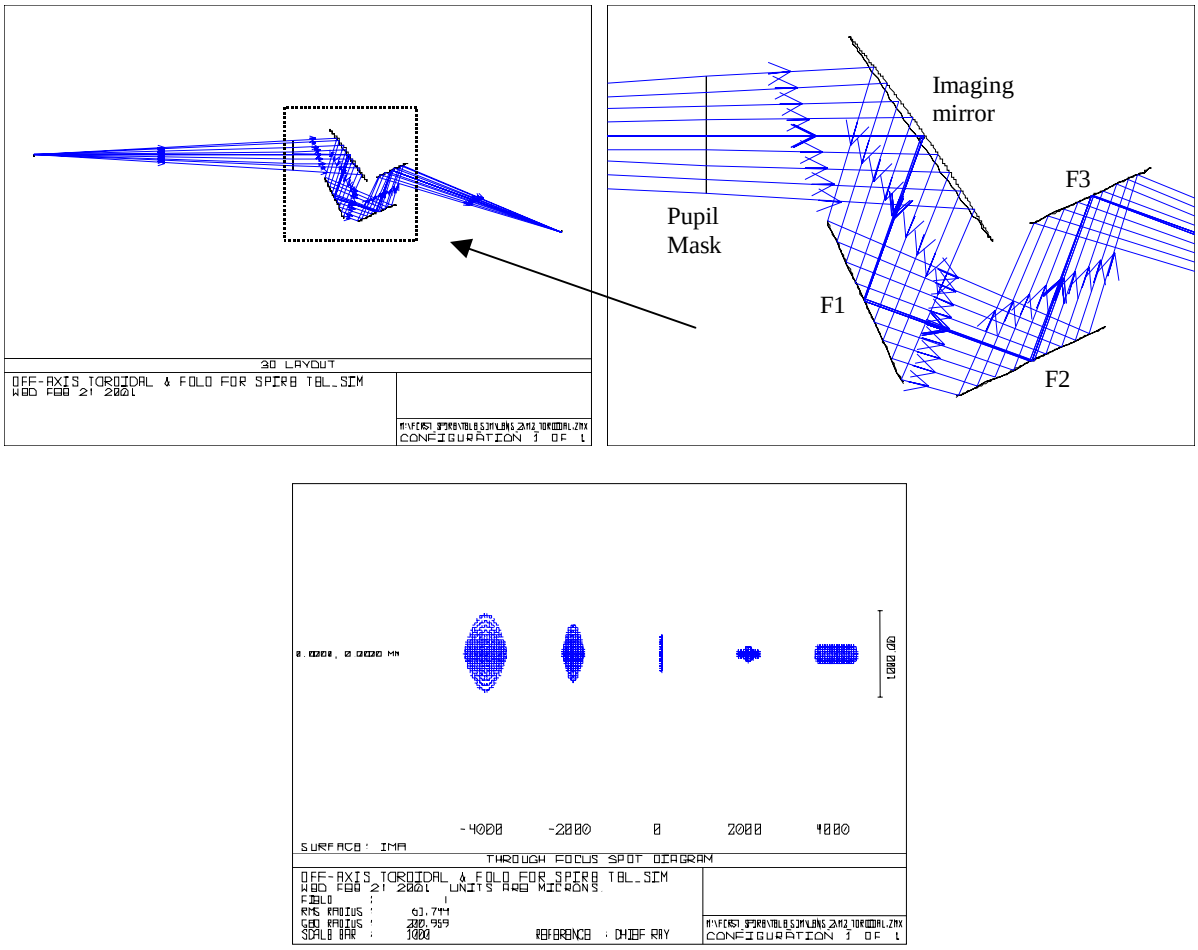

Figure 3: Zemax ray-tracing layout (yz plane) and spot diagrams for a configuration with i=35deg

4. Alignment consideration

The previous discussion shows the necessity to work with an off-axis angle of at least 35deg and no more than 45deg. An angle of 45deg seems to be better suited as it can be set with the use of a pentaprism. This will replace the first concept of locating foci of the mirror illuminating it on-axis then rotating it as the mirror (any of the 2 shape considered above) demonstrates poor optical imaging properties on-axis (too "slow" optics). A more detailed (step by step approach) alignment plan is under investigation and just a first possible draft concept is described below.

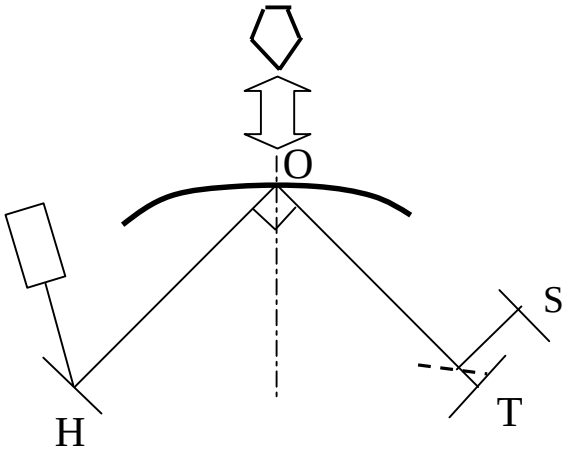

The visible laser + plate with hole (H) and the flat transfer mirror (T) can be set with reference to the optical bench (main level reference for the plane of propagation) with an autocollimator.

The pentaprism is used to set a 90deg angle between the incident and reflected beam. Then the pentaprism is replaced by the mirror. Assuming existence of a mark locating the centre O of the mirror, the 3 points O, H and impact on T should be in the same plane. Verification could be made by use of a beam splitter + image surface to locate the second conjugate focus S (and tilt angle errors) after moving H along the path OH (measured distance; no need to it for OT) to the required R_{SM} (first focus point) distance (use of slide radius with expected accuracy smaller than 1mm). This required the visible laser signal to be strong enough (not too much scattered by mirror surface roughness and consequently there is a need for extra polishing around the centre of the mirror). Fine-tuning for the focus at detector plane could be made afterwards when inserting the 3 fold mirrors system that would allow final correction/adaptation of the second focus to detector. All this is actually placed under constrain of space made available (mainly determined by the chosen R_{SM} distance compared to the size of possible optical bench).

5. Specification of the mirror

From the considerations developed in the above paragraph, the case of an ellipsoidal mirror with a biconic surface seems to present to best optical properties with respect to the requirements and considering manufacturing difficulties which would be the same in both cases.

5.1. Mirror dimensions:

Mirror needs to be oversized with respect to the beam size on its surface to avoid loss by edge diffraction and spillover. A factor 1.2 (20% oversized) is applied as a compromise between a too large size difficult and costly to manufacture and minimising the introduction of diffraction losses.
On-axis the beam impact on the mirror would be circular with a diameter ~230 mm (also given by $\sim R_{SM}/F\#$). Therefore in the case presented in section 1, we have D_x=276 mm and D_y=390 mm (the dimension is longer along y due to the angle of incidence i=45deg in yz plane).

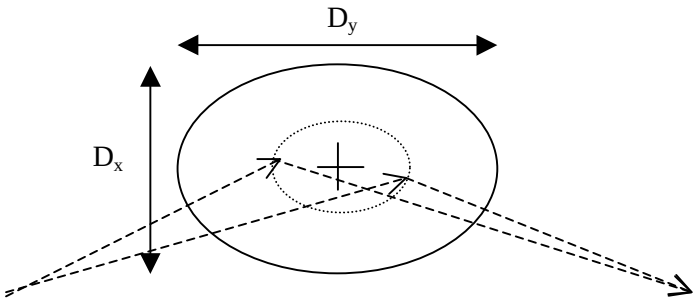

High precision is not particularly requested on these dimensions but would be driven by the manufacturing constraints[2]. The mirror thickness should be at least 10 mm (due to the surface definition, see below, and dimensions) at the edge but 10% of the mirror size is commonly used which leads in this case to ~30 to ~40 mm of thickness at the mirror aperture edge.
In order to reduce the mirror dimensions without changing the system parameters (R_{SM}, i), a 10% oversize factor only could be applied instead of 20% because the propagation is relatively well "beamed". A few percent loss may be expected through beam spreading due to diffraction over the free space optical path, which would affect mainly the longest working wavelength, as the diffraction coefficients varies with $\lambda^{1/2}$. This may need to be confirmed by further specific coherent beam pattern calculations. With this oversize smaller factor, the dimensions become D_x=252 mm and D_y=356 mm. These two sets of values would represent limits on the mirror dimensions for this value of R_{SM}. For lower values of R_{SM}, the mirror dimensions would decrease also as a good first-order estimation of the beam diameter of the mirror is given by R_{SM}/F#.

5.2. Surface definition:
The sag z of the biconic surface is given the following equation:

$$z = \frac{c_x x^2 + c_y y^2}{1 + \sqrt{1 - (1+K_x) c_x{}^2 x^2 - (1+K_y) c_y{}^2 y^2}}$$

with c_x=1/R_x and c_y=1/R_y and K_x=0, K_y=1, R_x=1400.64 mm and R_y=2801.29 mm. Tolerancing with Zemax showed that R_x and R_y should be vary no more than a few mm from these nominal values in order to keep a rms spot size radius smaller than 0.1 mm at the image point (particularly R_y). For the surface roughness, a max rms value taken as λ/20 can be used. With the smallest working wavelength at ~200 μm, that leads to ~10 μm rms which is well achievable even over the entire large surface area. For alignment purposes, the central part of the mirror (disk of a few cm in diameter around the middle) needs to be polished afterwards and should have a mark indicating the centre position. Cracks and surface defects may still remain after the polishing phase, and their sizes can cause some degradation (by surface scattering) of an alignment laser beam in the visible.

Different manufacturers have been approached and among them, Thomas Keating Ltd would be able to machine such a large optical component with the above specification. An expected delivery time was estimated to 8 to 10 weeks.

[2] The material is likely to be aluminium (lightweight, no corrosion) which leads to an approximate maximum weight of 6-7 kg for the mirror (excluding any support/mounting). With this metallic material (aluminium), a fractional power loss per reflection would be around 0.3% at λ~300μm.

5.3 Mechanical design:

From the above requirements and specifications, a mechanical drawing of the mirror was made. A PDF file of it can be found under the ref. RD7. A brief review of the drawing features is done here.

Apart from the front surface of the mirror based on the optical requirements, the back of the imaging mirror is designed from the following ideas (illustrated in Figure 4 below):

- the thickness should be at least ~10% of the longest dimension but should avoid interaction with rotating mirror F3,
- shape of the back should leave a clear zone for free-space beam propagation between F2 and F3 (inducing removal of the edge corners),
- a thick base (lowering the centre of gravity) is needed for stability in vertical position,

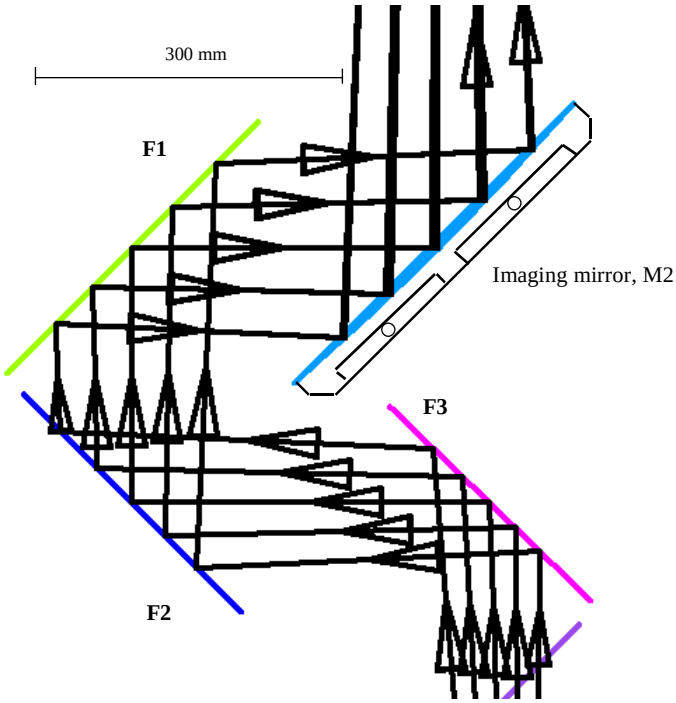

Figure 4: Zoom into the Telescope Simulator (ASAP model, optical layout plan view) with reverse (i.e. from simulated TFP) ray tracing in SPIRE FOV scan mode (large beam). M2 as from mechanical design is shown.

Extrusion of material in the back keeps the total weight less than about 15 kg. Bottom horizontal surface and lateral vertical ones are set to be reference for parallelism with the optical axis. They are designed within a tolerance limit obtained from alignment consideration (see RD8).

The elliptical aperture of the optical surface is enclosed in a larger (by ~4-5mm at the ellipse extremities) rectangular face (with final dimensions 285mm×400mm, 50mm maximum in thickness). This extra material is meant to be a margin allowing eventual re-machining of the surface (removing more material than expected) if not acceptable at delivery.

Verification of the surface shape can be performed by metrology measurements of the surface profile along X=0 and Y=0 axis, using bottom and lateral surfaces as references. These measurements will be limited in precision by the surface roughness (~10 μm) but should lead to the best-fitted profiles of the final shape along both planes of symmetries to a good accuracy. Parameters like the radii of curvature R_x and R_y can then be retrieved as well as the real position of the centre of the surface (possible deviation from the fiducial mark location) and the optical axis direction with respect to reference surfaces.

6. First-order (i.e. fundamental mode) Gaussian beam analysis

One of the foreseen system sources positioned at the front focus is a FIR laser. Such a source could be modelled as a provider of a near-gaussian beam with a finite size at the focus. Following long-wavelength (gaussian beam) optics formulation in RD4, one can define a gaussian beam waist located at the front focus of the ellipsoidal mirror. From GO consideration (relatively large F# so slow beam), the mirror can be modelled in a first order approximation as an on-axis lens-type perfect phase transformer (see figure below).

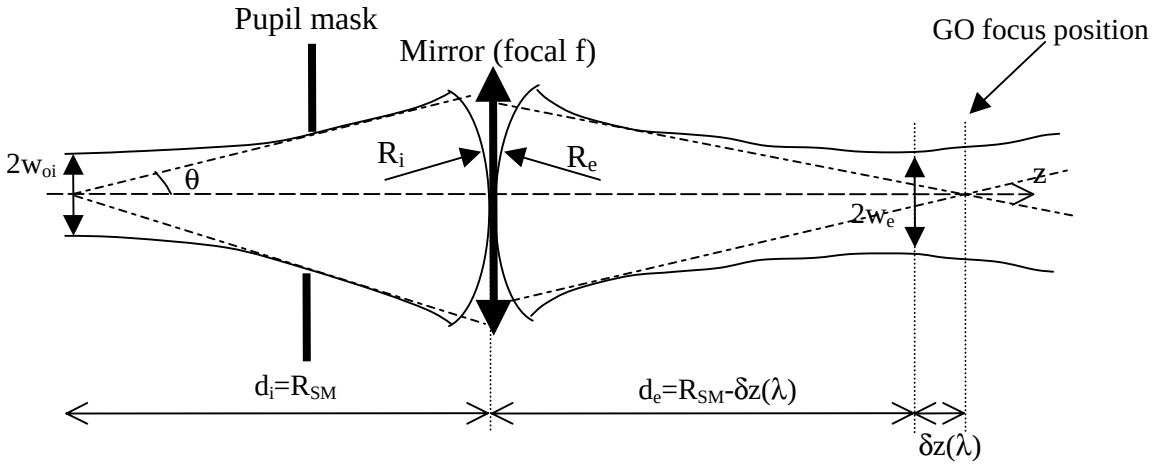

From GO analysis, a point source located at one of the ellipsoidal mirror foci (at R_{SM} from the mirror centre in this case) would be (perfectly) imaged at the conjugate focus, located at R_{SM} after the mirror. Extension of the analysis into Gaussian optics allows taking into account the effect of finite (long) wavelength. An incoming beam with a waist w_{oi} located at d_i from the mirror would give rise to a wavefront radius of curvature (ROC) R_i when reaching the mirror, with R_i given by:

$$R_i = d_i\left(1+\left(\frac{z_0}{d_i}\right)^2\right) = d_i + \left(\frac{\lambda^2}{\pi^2\theta^4 d_i}\right) \text{ where the confocal distance } z_0 \text{ is: } z_0 = \frac{\pi w_{oi}^2}{\lambda} = \frac{\lambda}{\pi\theta^2}$$

One can see that the ROC from a diffractive gaussian beam would differ by an additive term increasing with the wavelength from the expected GO spherical wavefront with ROC d_i. Applying the lens equation $1/f=(1/R_i)-(1/R_e)$ to obtain the emerging wavefront ROC from the mirror, and developing Re in the same as above as a function of d_e, would lead to a second-order equation in d_e. This result can be directly obtained from the transfer matrix (see RD4) between the initial beam size (radius w_{oi}) and divergence θ at d_i before the mirror to a plane at de after the mirror. In this case, one can directly get:

$$d_e = f + \frac{f^2(d_i - f)}{(f-d_i)^2 + \left(\frac{\pi w_{oi}^2}{\lambda}\right)^2}$$

Using the system parameters $d_i=R_{SM}$ and $f=R_{SM}/2$, d_e can be expressed in the following way:

$$d_e = \frac{R_{SM}}{2}\left(1+\frac{1}{1+\left(\frac{2\lambda}{\pi\theta^2 R_{SM}}\right)^2}\right) \approx R_{SM} - \delta z(\lambda)$$

where from first-order series development the wavelength-dependent defocus term is given by:

$$\delta z(\lambda) = \frac{2\lambda^2}{\pi^2 \theta^4 R_{SM}}$$

With R_{SM}=1980.81mm and an initial beam divergence[3] θ~1/2F# (with F#=8.68 => θ=0.0572rad), this longitudinal shift will be:

λ (μm)	**δz (mm)** with θ=0.0572rad	**δz (mm)** with θ=0.051rad
250	0.57	0.91
500	2.30	3.70

It should be noted that this effect would occur for the Herschel telescope and lead to focus re-positioning of the SPIRE detector feedhorns for optimum coupling (see details in RD5). In order to compensate for this effect at the telescope simulator level, the system source could be shifted longitudinally depending on the working frequency. Practically, the compensation can be achieved after the imaging mirror by moving together the mirrors F1 and F2. Such changes in the optical path length have already been studied in the focus control of the telescope simulator control laws where corrections of the order of a millimetre should be made during scan of the field-of-view (see RD2).

The large off-axis angle (i=45deg) could be a source of beam distortion as studied in RD6. From an incident fundamental-mode-gaussian-beam (FMGB), the emergent distorted beam is given in a first-order approximation by the following correction from an ideal emergent gaussian beam:

$$E_e(x_e, y_e, z_e = d_e) \propto \left(1 - \frac{\tan(i) w_e}{f}\left(\frac{x_e}{w_e} - \left(\frac{x_e}{w_e}\right)^3 - \left(\frac{x_e}{w_e}\right)\left(\frac{y_e}{w_e}\right)^2\right)\right) \cdot E_{e\_ideal}(x_e, y_e, z_e = d_e)$$

with the beam radius at d_e given by:

$w_e \approx w_{oi}\left(1 - \frac{2\lambda^2}{\pi^2 \theta^4 R_{SM}^2}\right) = \frac{\lambda}{\pi\theta}\left(1 - \frac{\delta z(\lambda)}{R_{SM}}\right)$, which is here very close to the input waist size. A graphical illustration of it is displayed on the figure below.

The loss of power from the fundamental is thought to transfer into higher-order modes and is estimated by $(1-\eta) \approx \frac{1}{8}\tan^2(i)\left(\frac{w_m}{f}\right)^2 \sim \frac{1}{8F\#^2}$ leading to value <0.2% for the present case (and w_m being the beam radius on the mirror). For the case of an incident polarised beam, twice this amount is thought to be transferred into cross-polar component after reflection on the off-axis mirror.

[3] One can see that δz is strongly dependent on θ. Here the value comes from GO consideration of rays limitation by the pupil mask dimensions and leads to an edge taper of -8.686dB (intensity level at $1/e^2$) at the pupil mask aperture edge. In RD1, a value of 0.051rad was used from Hershel telescope geometry and gaussian beam optics which would lead here to a larger magnitude of the edge taper (actually ~-10.91dB) and ~60% longer defocus δz. This value of θ=0.051rad is derived from a model of optimum coupling (overlap integral calculation) between a FMGB and an uniformly distributed field ("top-hat") across a circular aperture (the system pupil, i.e. Herschel secondary, or equivalently, in the Telescope Simulator case, the pupil mask). If the ratio "aperture radius/waist" is about 1.121, an optimum power coupling of 81.5% can be achieved in theory. Over-illumination of the pupil mask (θ>1/2F#) would bring the opposite effect. But these above values in δz are expected to be a worst-case estimation, as beam truncation by the pupil mask aperture would bring the global system behaviour closer to GO results.

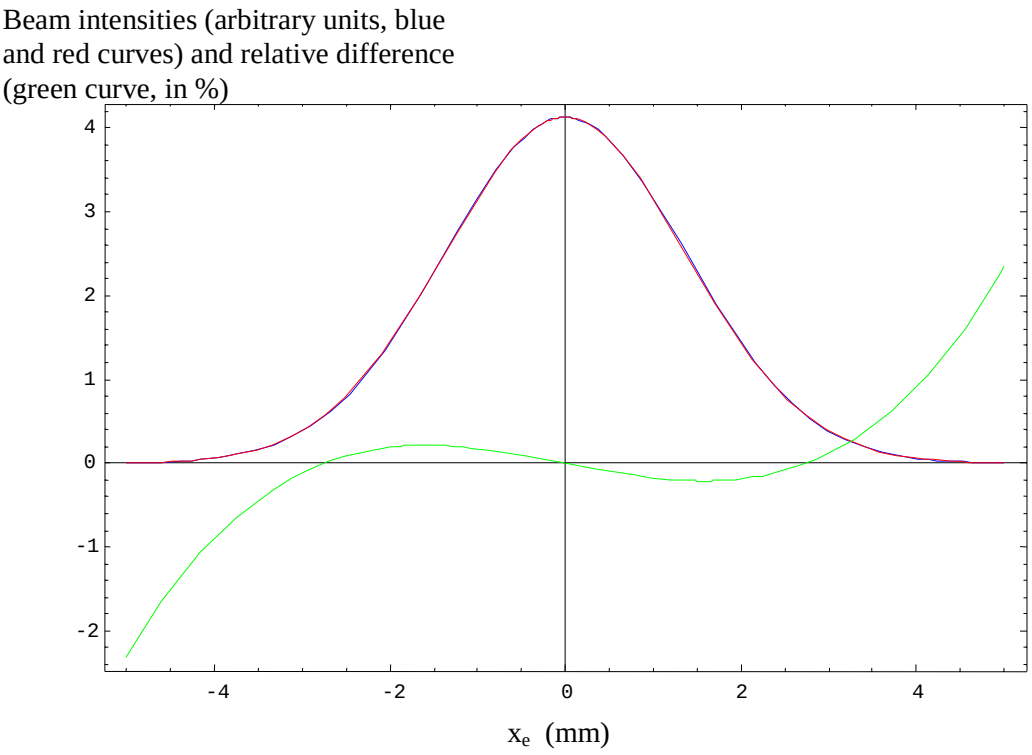

Figure 5: Intensity for an ideal gaussian beam (blue), a real distorted beam (red) and their relative difference in % (green) as function of x_e (in mm) in the plane $y_e=0$, $z_e=d_e$.

All these quantitative estimations show effects with quite small magnitude. Deviations, other than the ones due to above approximation, may arise from beam clipping effect at the pupil mask and real field distribution at the source (higher-order gaussian modes for example).